Applied Energy 282 (2021) 116134

Contents lists available at ScienceDirect

Applied Energy

journal homepage: www.elsevier.com/locate/apenergy

Effect of pilot fuel properties on lean dual-fuel combustion and emission characteristics in a heavy-duty engine

Zeeshan Ahmad *, Ossi Kaario, Cheng Qiang, Martti Larmi

Department of Mechanical Engineering, Aalto University School of Engineering, 02150 Espoo, Finland

HIGHLIGHTS

- Lean methane dual-fuel combustion with a small pilot quantity.
- Identification of dual-fuel combustion stages based on the second derivative analysis.
- Cetane number, a most significant pilot fuel property improving combustion efficiency.
- Aromatic content may help to reduce exhaust emissions at an expense of high NO_x.
- High volatility may lead a pilot spray to lean out within premixed methane-air mixture.

ARTICLE INFO

Keywords:
Cetane number
Aromatic content
Dual-fuel emissions
Combustion analysis
Injection pressure
Engine speed

ABSTRACT

In a dual-fuel (DF) combustion process, the ignition of the main fuel plays a crucial role on engine performance and emissions. In the present work, a pilot fuel is used to ignite a gaseous methane-air mixture. Three diesel-like pilot fuels are used comparing especially the cetane number (CN) and the aromatic content (AC). The experiments are conducted in a single-cylinder heavy-duty research engine keeping the total-fuel energy constant. Lean conditions are applied for the port-fuel injected methane-air mixture ($\varnothing_{CH4} = 0.52$). The methane provides 97% of the total energy while 3% of the energy comes from a pilot fuel. The experiments are performed for two pilot-fuel injection pressures and two engine speeds. The results of the present work suggest that DF combustion consists of three overlapping combustion stages: (**I**) ignition of the pilot fuel, (**II**) burning of the main fuel in the vicinity of the pilot fuel, and (**III**) combustion of the remaining main fuel. It was observed that cetane number directly affects the peak heat-release rate (HRR_{peak}) during Stage **I**, whereas aromatic content influences HRR_{peak} during Stages **II** and **III**. A fuel with high cetane number and aromatic content provides high DF combustion efficiency, low methane slip, THC and CO emissions at the expense of high NO_x emissions. An increase in the aromatic content is responsible for the increased NO_x emissions. Based on the average performance trends of the pilot fuels, they can be rated as [high CN, high AC] > [Low CN, high AC] > [High CN, AC free].

1. Introduction

In recent years, the use of low-carbon gaseous and liquid biofuels has gained popularity in the transport sector in order to meet stringent regulations on engine-out emissions [1–3]. This has resulted in a stunning increase in global biofuel production at an average rate of 14.8% per annum [1,4]. However, this growth was only enough to cover 3.7% of the transport-fuel demand in 2018 [5]. Moreover, according to the International Energy Outlook (IEA), the global transport-fuel demand has continued to grow at an annual rate of 1.4% [5]. Consequently, the goal to meet greenhouse-gas (GHG) emission target in the transport sector has led to the electrification of light-duty vehicles in the first phase [6]. However, diesel engines seem to remain the prime mover for heavy-duty transport, especially maritime transport sector for the coming decades. Maritime transport accounts for nearly 80% of the worldwide trade, which is responsible for about 2.5% of the global GHG emissions [6,7]. In addition, heavy-duty transport produces about 25% of the global GHG emissions [6,7]. In this scenario, in addition to increasing the consumption of various biofuels, fuel-efficient and less polluting diesel engines utilizing advanced combustion technologies have become an important research topic.

Dual-fuel (DF) combustion is an advanced low-temperature combustion (LTC) strategy [8], employing various alternative fuels in

* Corresponding author.
E-mail address: zeeshan.ahmad@aalto.fi (Z. Ahmad).

https://doi.org/10.1016/j.apenergy.2020.116134
Received 13 March 2020; Received in revised form 26 October 2020; Accepted 27 October 2020
Available online 12 November 2020

Nomenclature

DF	Dual fuel
gIMEP	Gross indicated mean effective pressure
TDC	Top-dead center
CAD	Crank angle degree
ATDC	After top-dead center
HRR	Apparent heat-release rate
HRR_{peak}	Peak heat-release rate
SDHRR	Second derivative of heat-release rate
AccQ	Accumulative heat release
TFE	Total injected fuel energy
LHV	Lower heating value
AFR	Air to fuel ratio
PF	Pilot fuel
CN	Cetane number
AC	Aromatic content
UB-CH_4	Unburned methane or methane slip
THC	Total unburned hydrocarbons
CO	Carbon monoxide
NO_x	Nitrogen oxides
CO_2	Carbon dioxide
I	First stage combustion
II	Second stage combustion
III	Third stage combustion
P_R	Pilot ratio
P_{PF}	Pilot-fuel injection pressure
ω	Engine speed
P_{air}	Charge-air pressure
MP_{peak}	Motored peak pressure (only air)
T_{air}	Charge-air temperature
T_{TDC}	Calculated isentropic temperature at TDC
T_{10}, T_{50}, T_{95}	Distillation temperatures
$\dot{m}$	Mass flow rate
$\varnothing_{CH4}$	Methane equivalence ratio
η_{comb}	Combustion efficiency
η_{th}	Thermal efficiency
$\eta_{indicated}$	Gross indicated efficiency
t_{ID}	Ignition-delay time
t_{comb}	Combustion duration
t_{CAD}	Available time per CAD
θ_{SOI}	CAD at start of injection
θ_1, θ_2, θ_3	CAD at start of combustion stages
θ_{3a}, θ_{3b}	CAD at start of high-, low-intensity regime of Stage **III**
θ_{90}	CAD where 90% of total heat releases
C_{input}	Total carbon content of injected fuel

existing diesel engines [9–11]. Several commercially operated examples of DF engines have already been adopted by the shipping and power generation industry. These engines use two fuels of different reactivity, in which a directly injected high-reactivity pilot fuel (PF) ignites a port-injected low-reactivity fuel close to the top-dead center (TDC) [9,10]. The high-reactivity pilot fuel is usually a conventional diesel or diesel-like fuel (biofuel). On the other hand, the most employed low-reactivity fuel in DF engines is natural gas (NG) due to its abundance and worldwide availability at a low price. Furthermore, methane (the main constituent of NG) is a low-carbon fuel, which inherently produces less carbon dioxide (CO_2) than other hydrocarbons [9,11,12]. In general, diesel-methane DF engines provide higher thermal efficiency (η_{th}) than conventional diesel engines at high loads [13]. Additionally, they produce lower nitrogen oxides (NO_x), particulate matter (PM) [8,14,15] and close to zero sulfur oxides (SO_x) [16], while utilizing small pilot quantities to burn a lean premixed methane-air mixture [17]. However, under lean conditions, this may induce combustion instabilities [18,19] and lead to significant emissions of carbon monoxide (CO) [20] and unburned methane or 'methane slip' (UB-CH_4) [12,16,21]. Despite the advantages of DF engines over conventional diesel engines, the UB-CH_4 from DF engines is a major concern, as UB-CH_4 has dramatically higher global warming potential than CO_2 over a long-term perspective [16,21–23]. It is therefore important to further develop the lean DF combustion process in order to meet future stringent emission regulations.

Many researchers have investigated various biofuels in DF engines in order to improve efficiency and achieve reduced engine-out emissions. Namasivayam et al. [24,25] studied natural gas DF combustion by employing three PFs, such as conventional diesel, rapeseed methyl ester (RME), and dimethyl ether (DME). The results show a similar level of engine-out emissions for RME and conventional diesel due to similar physical and chemical properties. However, RME is reported to produce higher THC at higher engine speed as a result of incomplete combustion. On the other hand, DME produced lower NO_x with higher CO and THC than RME at low load and higher engine speed due to incomplete combustion. Bora et al. [26] compared three methyl-ester (ME) PFs produced from three different feedstocks (i.e., rice-bran oil, pongamia oil, and palm oil) in a biogas run DF engine at different loads. They found that rice-bran ME shows the highest efficiency and NO_x accompanied by the lowest CO emissions among all PFs. Tira et al. [27] studied conventional diesel, RME and gas-to-liquid (GTL) PFs in a port-fuel injected (PFI) liquefied-petroleum gas (LPG) DF engine. They reported a significantly reduced NO_x-soot emission trade-off for GTL among all three fuels. RME showed better engine performance in terms of combustion variability, total-unburned hydrocarbons (THC), CO, and soot than conventional diesel. On the other hand, GTL resulted in lower NO_x over a wide range of engine operating conditions due to its high cetane number (CN) and absence of aromatics. Similarly, other researchers [28–32] have compared conventional diesel with various biodiesel PFs in DF engines. These studies reported either similar or different trends for thermal efficiency and engine-out emissions. Nevertheless, they found that biodiesel can replace the conventional diesel in DF engines.

Although previous literature has discussed various PFs in DF engines, most of these studies have discussed the fuel properties rather tentatively. Only a few studies [33–35] have attempted to evidently explain the effect of PF properties on DF combustion. Ansari et al. [33] investigated two diesel-like PFs of different CN in a NG run DF engine in RCCI mode. Their results showed that CNs is the most significant factor

Table 1
Specifications of the research engine.

Engine type	4 stroke, modified single-cylinder DF engine		
Piston geometry	Re-entrant bowl		
Displacement volume	1.4 L		
Bore × Stroke	111 × 145 mm		
Geo. compression ratio	16.7:1		
In-cylinder swirl ratio	2.7		
Pilot injection system	Bosch common rail with piezoelectric injector		
Injector no. of holes × diameter	3 × 0.160 mm (symmetric)		
Port fuel injection system	2 × EG2000 gas injectors		
Firing TDC	0 CAD ATDC		
Valve timing		Inlet	Exhaust
	Opening time	356 CAD ATDC	150 CAD ATDC
	Closing time	−155 CAD ATDC	−340 CAD ATDC

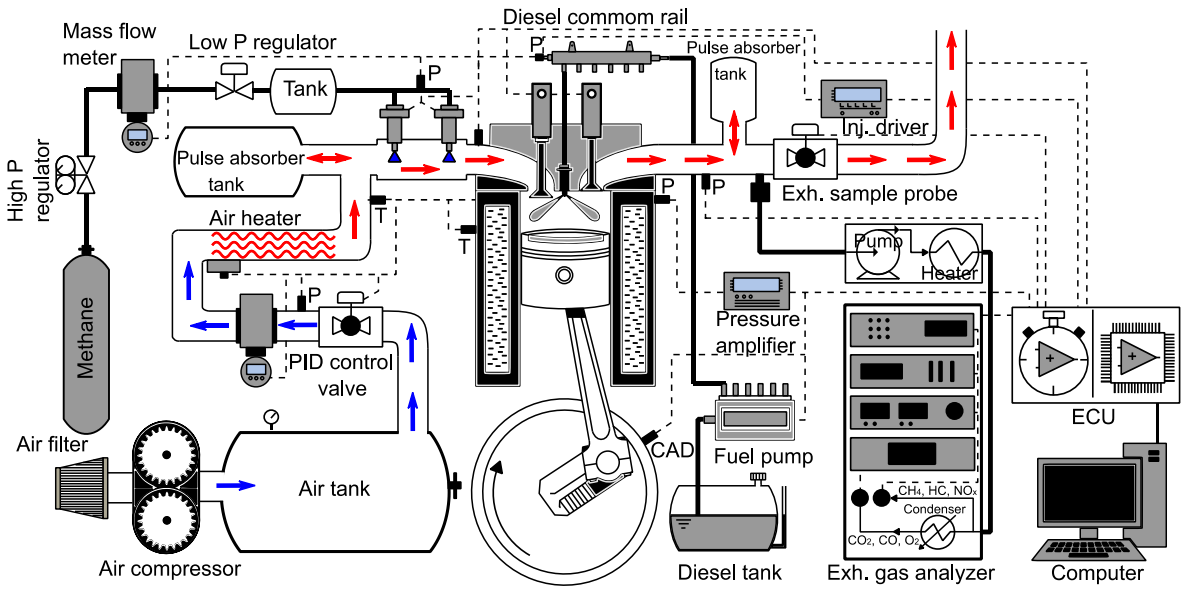

Fig. 1. Schematic of the research-engine laboratory setup and emission analyzing system.

affecting THC and CO emissions. High CN fuel provides higher thermal efficiency, reduced THC and reduced coefficient of variability. Chuahy et al. [34] investigated two PFs of different volatility in an RCCI operated engine both experimentally and numerically using port-fuel injected iso-octane. They found that the difference in volatility has a minimal effect on the combustion.

Despite the importance of the contributions from these studies, a little is known about the various PF properties affecting DF combustion. Moreover, the knowledge from conventional diesel combustion [36–38] cannot be categorically applied to predict DF combustion behavior due to a complex interaction between two fuels. Therefore, the present work addresses this gap by investigating three diesel-like PFs with different physical and chemical properties in a single-cylinder DF research engine. Thus, the main objectives of the present work are,

1. to define the DF combustion stages from heat release rate (HRR) profiles at different engine conditions,
2. to demonstrate the influence of pilot-fuel injection pressure (P_{PF}) and engine speed (ω) on lean DF combustion characteristics and engine-out emissions,
3. to explain the influence of pilot fuel CN, total aromatic content (AC), and various physical properties on lean DF combustion characteristics and engine-out emissions, as well as
4. to demonstrate a combined effect of different properties (e.g. CN and AC) in order to identify the dominant fuel properties.

2. Experimental setup and procedure

2.1. Research engine

The research engine used for the experiments is a heavy-duty diesel engine modified for single-cylinder dual-fuel operations. The specifications of the engine are summarized in Table 1, and a schematic of the laboratory engine setup is shown in Fig. 1. The engine allows monitoring and flexible control of engine operating parameters related to necessary parallel systems, such as electro-hydraulic valve actuation (EHVA), charge-air conditioning, and fuel injection systems. The EHVA system enables camshaft-less valve actuation with flexibly adjustable valve timings and lifts [39]. The engine is equipped with RHM-08 and RHM-015 Coriolis mass flow meters (Rheonik Messtechnik GmbH), for measuring charge-air ($\dot{m}_{air}$) and port-injected methane mass flow rates ($\dot{m}_{CH4}$), respectively. A port-fuel injection system containing two gas injectors supplies methane into the intake manifold during the intake stroke along with the charge air. Similarly, a common rail direct-injection system containing a 3-hole piezoelectric injector directly delivers PF into the cylinder with an ability to control the injection timing and the quantity of the PF. The piezoelectric injector provides a microsecond environment, thereby enabling shorter injection durations and smaller PF quantities than can be delivered by a conventional solenoid injector. Furthermore, the engine is equipped with a Kistler model 5011 charge amplifier for measuring in-cylinder pressure at a resolution of 0.2 CAD.

The engine is provided with an emission-analyzing system consisting of various analyzers for each gas. An exhaust sampling probe directly extracts a sample of raw emission gas and delivers it to emission analyzers. A heated-flame ionization detection (HFID) based analyzer Model VE-7 (J.U.M Engineering GmbH) measures THC. The CLD-822Sh (ECO Physics AG) analyzer based on chemiluminescence measures NO_x emissions. Two SIDOR non-dispersive infrared spectroscopy (NDIR) based analyzers (Sick AG) are employed to measure UB-CH_4, CO, and CO_2. In addition, a paramagnetic dumbbell (OXOR-P) analyzer (Sick AG) measures oxygen content (O_2) in the raw emission gas. In general, all systems are electronically instrumented with the electronic engine control unit (ECU) based on the national instrument field-programmable gate array (NI-FPGA), which controls the engine and performs high-speed data acquisition at 40 MHz.

2.2. Test fuels

In the present work, 99.9% pure methane and three diesel-like liquid fuels of CN between 43 and 56, and AC of 0–22% are used as test fuels. Methane is adopted as the port-injected main fuel, while liquid fuels are employed as direct-injected PFs. The properties of the PFs are custom designed in such a way that two fuels have similar CN but have dissimilar AC and vice versa. The PFs are mainly composed of paraffins, naphthenes and aromatic hydrocarbons, though they contain no olefin. The varying proportions of these hydrocarbons in a fuel govern distinct physical and chemical properties. The detailed properties of the pilot fuels (PF1, PF2, and PF3) are listed in Table 2. The PFs are ultra-low sulfur fuels, which satisfy the ASTM D975 standard specification.

Table 2
Test fuels physical and chemical properties.

Fuel Properties	PF1	PF2	PF3	Methane
Molecular formula	C_9–C_{21}	C_9–C_{18}	C_9–C_{21}	CH_4
Derived cetane number (CN) (Std. – DIN EN-15195)	43.3	56.0	54.7	–
Paraffins [wt.%]	37.0	45.1	45.8	–
n-paraffins	17.0	15.2	17.2	–
Iso-paraffins	19.9	29.9	28.8	–
Naphthenes [wt.%]	40.7	54.9	33.9	–
Total aromatic content (AC) [wt. %]	22.3	<0.1	20.3	
Mono-aromatics [wt.%] (Std. – DIN EN-12916)	19.19	–	18.17	–
Di-aromatics	3.01	–	2.03	–
Tri-aromatics	0.11	–	0.08	–
Polyaromatics (PAH)	3.12	–	2.11	–
T_{10} [°C] (Std. – ASTM D7213 Cryo)	172.4	183.6	190.0	–
T_{50} [°C]	223.6	243.7	278.9	–
T_{95} [°C]	314.9	322.2	371.5	–
Density [kg/m^3]	824.4	810.2	829.2	0.656
Dynamic viscosity [mPa·s] @ 30 °C	1.7	2.16	2.95	0.0112
Kinematic viscosity [mm^2/s] @ 30 °C	2.06	2.66	3.56	17.07
Lower heating value (LHV) [MJ/kg]	43.31	42.25	43.37	50
Carbon content [wt.%]	86.21	85.94	86.13	74.86
Hydrogen content [wt.%]	13.79	14.06	13.87	25.14
A/F ratio (mass-based)	14.5	14.4	14.47	17.19
Auto-ignition temperature [°C]	250–350	250–350	250–350	600

The lower heating values (LHVs) of the PFs are similar; however, a difference in LHVs generally affects a volume consumption of a fuel mixture. The spray characteristics and the fluidity[1] of a fuel are most significantly affected by three main properties: viscosity, density, and volatility [36,40–43]. These thermophysical properties influence interactions between diesel spray and premixed methane-air mixture. Lower viscosity contributes to homogenous mixing by improving atomization and causing smaller fuel droplets (lower spray penetration and wider spray cone angles). On the other hand, higher viscosity reduces atomization and causes stratified mixing. In general, the density of a fuel is related to spray liquid penetration, while lower density causes smaller fuel droplets. Volatility refers to the rate of vaporization, which is defined by the distillation temperatures of the fuel as T_{10}, T_{50}, and T_{95}, where T_{10} denotes the temperature at which 10% of the fuel mass is evaporated, with heavier hydrocarbons usually evaporating at higher temperatures [36,40–43]. Overall, this implies that higher viscosity, density, and distillation temperatures typically lead to larger fuel droplets.

Furthermore, since fuel density and viscosity are strongly correlated, it is difficult to discern the effect of either property on combustion [36,40–43]. Nevertheless, where necessary, the effect of thermophysical properties on DF combustion will be explained in Section 3.

2.3. Operating conditions and procedures

In this work, total-fuel energy (TFE) is kept constant for all investigated test-points, wherein 97% of the TFE is contributed by methane as the main fuel. The remaining 3% of the TFE is supplied by a PF. Methane is injected into the intake manifold by gas injectors at −355 CAD ATDC during the intake stroke, which is ignited by a PF directly injected at θ_{SOI} = −7 CAD ATDC. During the experiments, the test fuels are injected only after achieving stable operating conditions. Table 3 shows the operating conditions that are kept constant for all investigated test points. The charge-air temperature (T_{air}) is adjusted in order to obtain the isentropic-compression temperature at firing TDC (T_{TDC}) of 835 K, as calculated by Eq. (1). In addition, the charge-air is fed into the cylinder at a boost pressure (P_{air}) to achieve a constant motored-peak pressure (MP_{peak}) of 60 bar, while simultaneously maintaining the charge-air mass flow rate ($\dot{m}_{air}$) at a value resulting in a methane equivalence ratio ($\varnothing_{CH4}$) of 0.52. For the pre-engine-run condition, the cylinder head and the liner of the engine are preheated through the water jacket to 353 K.

[1] The PFs have viscosities within the lower and upper designed limits of the common rail direct-injection system, therefore, hydrodynamic effect of viscosity on the injection system can be neglected.

Table 3
Summary of operating conditions.

Engine speed (ω) [rpm]	950, 1500
Pilot injection Pressure (P_{PF}) [bar]	1000, 1500 bar
Motored isentropic temperature at TDC (T_{TDC}) [K]	835
Motored peak pressure (MP_{peak}) [bar]	60
Methane equivalence ratio ($\varnothing_{CH4}$)	0.52 ± 0.01
Methane substitution ratio	97%
Pilot ratio (P_R)	3%
Pilot injection timing (θ_{SOI})	−7 CAD ATDC
Total fuel energy per cycle (TFE) [J/cycle]	3300 ± 100

In order to record a reliable test data along with averaged exhaust emission data, each test point is continuously run for 5 min after injecting test fuels. The in-cylinder pressure data is averaged over 100 successive combustion cycles for each test point, and undesired noise from raw-pressure data is filtered by employing a low-pass Butterworth filter algorithm. Based on the first law of thermodynamics, averaged pressure data is used to calculate the apparent heat release rate (HRR) and accumulative heat released (AccQ) for each test point using Eqs. (2) and (3), respectively [44]. In addition, pilot ratio (P_R) and methane equivalence ratio ($\varnothing_{CH4}$) of the charge are calculated using Eqs. (4) and (5), respectively. The engine-out emissions are converted from ppm to g/kWh based on stoichiometry [44]. The combustion efficiency (η_{comb}) is calculated using Eq. (6).

$$T_{TDC} = T_{air} \times \left(\frac{MP_{peak}}{P_{air}}\right)^{\gamma-1/\gamma} \tag{1}$$

$$\text{HRR} = \frac{dQ}{d\theta} = \frac{\gamma}{\gamma-1} P \frac{dV}{d\theta} + \frac{1}{\gamma-1} V \frac{dP}{d\theta} \tag{2}$$

$$\text{AccQ} = \int \frac{dQ}{d\theta} d\theta \tag{3}$$

$$P_R = \frac{\dot{m}_{PF} \times LHV_{PF}}{\dot{m}_{PF} \times LHV_{PF} + \dot{m}_{CH4} \times LHV_{CH4}} \tag{4}$$

$$\varnothing_{CH4} = \frac{(AFR_{CH4})_{stoichiometric}}{\left(\dot{m}_{air}/\dot{m}_{CH4}\right)_{actual}} \tag{5}$$

$$\eta_{comb} = \frac{CO_2}{Total\ C_{input}} \times 100 \tag{6}$$

2.3.1. Energy balance

A detailed energy balance analysis represents the actual improvement in engine performance. It identifies the total-fuel energy distribution into various energy losses such as combustion, heat transfer, exhaust and pumping losses. Here, the energy balance analysis is performed using the first law of thermodynamics. The pumping losses ($E_{pumping\ loss}$) are determined as a difference between net and gross indicated efficiencies [44,45]. The gross indicated efficiency ($E_{indicated\ work}$) is calculated using Eq. (7). The net and gross indicated mean effective pressures (*nIMEP*, *gIMEP*) are calculated for intervals;

Table 4
Summary of the cases and considered main PF properties for comparison (see detailed PF properties in Table 2).

PF type	CN	AC [wt.%]
Case A: *effect of CN*		
PF1	43.3	22.3
PF3	54.7	20.3
Case B: *effect of AC*		
PF2	56.0	<0.1
PF3	54.7	20.3
Case C: *combined effect of CN and AC*		
PF1	43.3	22.3
PF2	56.0	<0.1

−360 to 360 CAD ATDC and −180 to 180 CAD ATDC, respectively [44,45]. Likewise, the combustion losses ($E_{unburned\ fuel}$) are defined as a difference between total-fuel energy and combustion energy using Eq. (8). The exhaust losses ($E_{exhaust\ loss}$) are calculated using Eq. (9). Here exhaust gas is considered as a mixture of UB-CH_4, THC, CO_2, CO, NO, NO_2, N_2, O_2, and H_2O. The enthalpies of the charge air and exhaust gases are estimated using the Nasa Polynomials [44] at corresponding intake air (T_{air}) and exhaust gas temperatures ($T_{exhaust}$). The energy lost in heat transfer ($E_{heat\ transfer}$) is calculated by subtracting all above losses from total-fuel energy. Thus, the thermal efficiency is estimated according to Eq. (10).

$$E_{inidcated\ \ work} = \frac{gIMEP \times V_{displacement}}{TFE} \times 100 \tag{7}$$

$$E_{unburned\ \ fuel} = \frac{TFE - (\eta_{comb} \times TFE)}{TFE} \times 100 \tag{8}$$

$$E_{exhaust\ \ loss} = \frac{H_{exhaust} - H_{air}}{TFE} \times 100 \tag{9}$$

$$\eta_{th} = \frac{gIMEP \times V_{displacement}}{\eta_{comb} \times TFE} \times 100 \tag{10}$$

2.4. Test matrix

To demonstrate the effect of pilot-fuel properties on DF combustion, this work uses three case studies: effect of CN (Case A), effect of AC (Case B), and combined effect of CN and AC (Case C). The case studies are summarized in Table 4, and the experimental test points for each case are listed in Table 5. In each case, two pilot fuels are compared in order to determine the effect of a single PF property on DF combustion characteristics and engine-out emissions. However, in Case C, a combined effect of CN and AC is studied to determine the relative importance of either property on DF combustion. In addition, two different PF injection pressures (P_{PF}) and engine speeds (ω) are used to explore the effect of spray attributes and residence time on the combustion. The experimental test points are investigated under constant operating conditions, as described in Table 3. Furthermore, it is worth noting that at different ω, the operating conditions are kept constant by adjusting T_{air} and P_{air} in order to achieve constant T_{TDC} and MP_{peak}, while maintaining the same quantity of fuel and charge air per cycle.

2.5. DF combustion interpretation

Fig. 2 shows an example of the combustion stages identified for the two typical DF HRR profiles investigated in this study, as will be discussed in Section 3. The combustion stages θ_1, θ_2, and $\theta_3 = \theta_{3a} + \theta_{3b}$ along with θ_{90} are marked on the DF HRR curves. In general, DF combustion progresses as a combination of three overlapping combustion stages, which are identified based on the second derivative of the heat release rate (SDHRR) analysis presented in our previous work [46]. θ_1 represents the start of the first-stage combustion (**I**), during which most of the pilot fuel burns in a premixed mode along with an entrained premixed methane-air mixture. Similarly, θ_2 shows the start of the second-stage combustion (**II**), wherein the premixed methane-air mixture burns in the vicinity of the ignited pilot-fuel plumes. During this stage, the pilot fuel burns as locally fuel-rich zones or in the diffusion mode, depending on P_R. The third stage (**III**) is depicted as θ_3 =

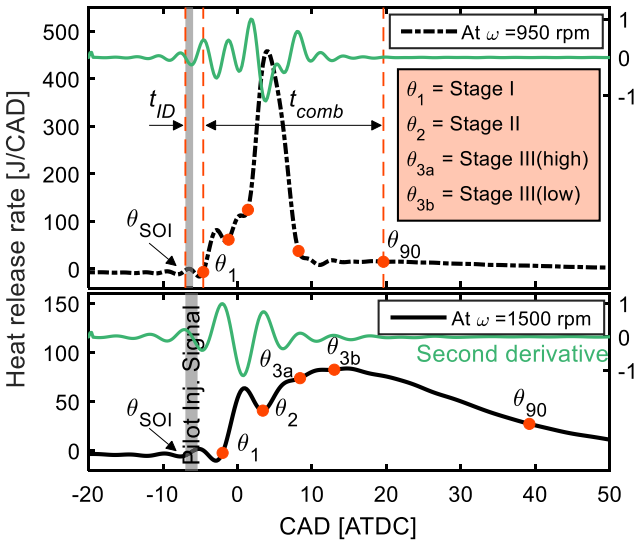

Fig. 2. An example showing the three overlapping DF combustion stages determined from typical HRR profiles investigated in this work. The stages are identified by the second derivation of HRR analysis. It is interesting to note that the profiles of the HRR curves tend to change from multi-peaks (M-shaped) to quasi-single peak with decreasing ω from 1500 rpm to 950 rpm.

Table 5
Test points and corresponding calculated performance parameters.

PF Type	ω [rev/min]	P_{PF} [bar]	$\dot{m}_{PF}$ [mg/cycle]	$\dot{m}_{CH4}$ [mg/cycle]	TFE [J/cycle]	gIMEP [bar]	η_{comb} [%]	η_{th} [%]
PF1	950	1000	2.38	66.1	3406.8	11.66	97.32	49.22
		1500		66.2	3417.4	11.86	97.79	49.70
	1500	1000	2.36	62.5	3224.4	10.50	89.33	51.05
		1500		62.2	3214.3	11.07	92.33	52.32
PF2	950	1000	2.38	66.1	3405.1	11.61	97.30	49.03
		1500		66.5	3431.4	11.73	97.73	48.95
	1500	1000	2.36	62.7	3241.1	10.73	90.17	51.43
		1500		62.7	3235.5	11.04	91.61	52.13
PF3	950	1000	2.38	66.3	3415.6	11.73	97.75	49.20
		1500		66.9	3445.2	11.98	97.97	49.65
	1500	1000	2.36	62.1	3203.3	10.50	89.13	51.47
		1500		62.7	3237.8	11.35	93.26	52.62

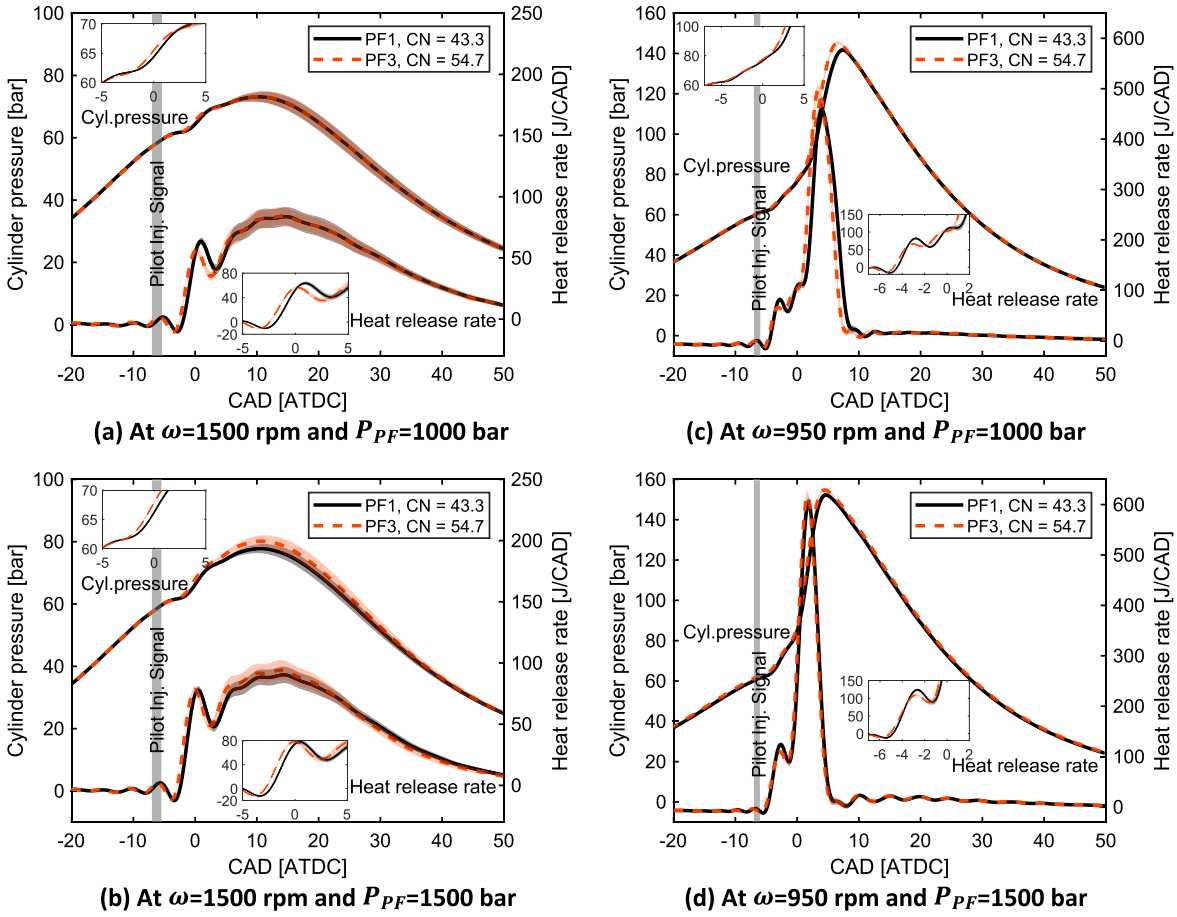

Fig. 3. Averaged cylinder pressure and heat release rate (HRR) data along with standard deviation at two different ω and P_{PF}. Two pilot fuels (PF1 and PF3) are compared to study the effect of CN on lean ($\varnothing_{CH4} = 0.52$) DF combustion.

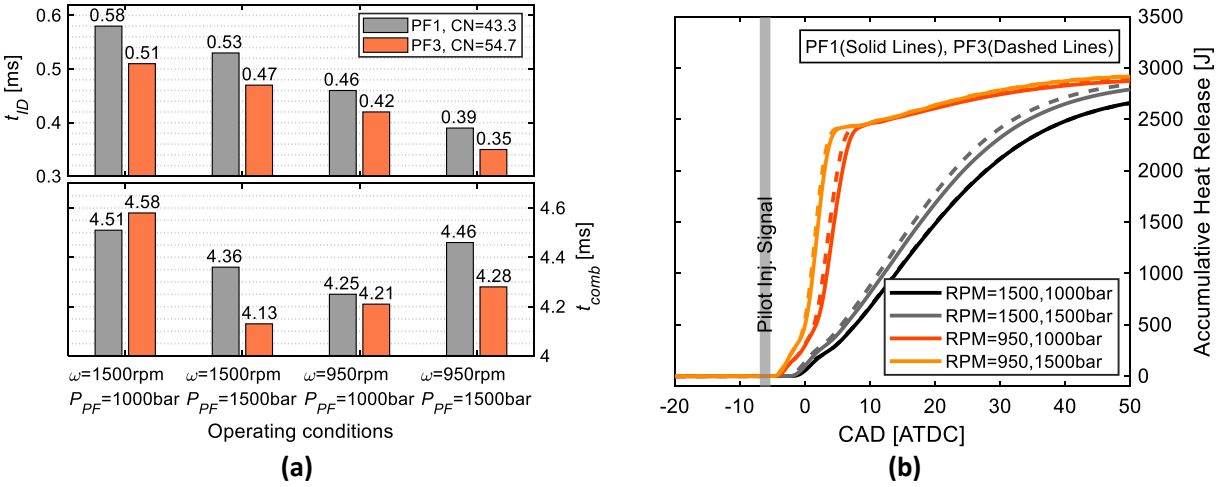

Fig. 4. (a) Ignition-delay time (t_{ID}) and combustion duration (t_{comb}), (b) accumulative heat released (AccQ) data for the study of effect of CN on lean DF combustion.

$\theta_{3a} + \theta_{3b}$, with θ_{3a} denoting the start of the third-stage combustion. During this stage, the remaining unburned premixed methane-air mixture burns in the turbulent-flame propagation mode, and rapidly releases heat during a high-intensity regime (between θ_{3a} to θ_{3b}) compared to a low-intensity regime (between θ_{3b} to θ_{90}), where HRR decreases due to dilution and quenching. Here, θ_{90} exhibits a CAD at which 90% of the total heat (AccQ) is released. Furthermore, in this work, ignition-delay time (t_{ID}) is defined as a time interval between θ_{SOI} and θ_1, whereas combustion duration (t_{comb}) is defined as a time interval between θ_1 and θ_{90} based on the SDHRR [46].

3. Results and discussion

This section discusses the results obtained from the experiments in

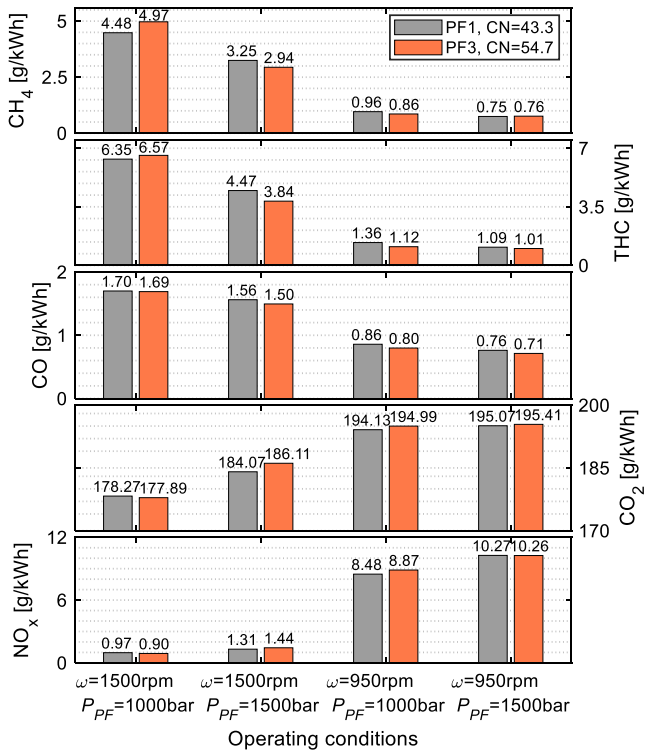

Fig. 5. Engine-out emission data for the study of effect of CN on lean DF combustion.

three case studies (Table 4). Each case study analyzes the aforementioned effects of PF properties on HRR and other DF combustion characteristics, such as t_{ID}, t_{comb} and engine-out emissions. The results are presented for two P_{PF} at two different ω in addition to constant operating conditions, as outlined in Table 3. Fig. 2 (Section 2.5) shows the typical DF combustion stages distinguished from similar HRR curves discussed below for different test points.

3.1. Case A: Effect of cetane number (CN)

The effect of cetane number on DF combustion is investigated by comparing PF1 and PF3 in Figs. 3–5. It is known that cetane number defines the ignition quality of a fuel, and a fuel with higher cetane number ignites earlier than a fuel with lower cetane number [35–37]. Accordingly, PF3 ignites earlier and depicts shorter ignition-delay time and combustion duration than PF1, as illustrated in Fig. 4(a). However, it is observed that PF1 with longer t_{ID} shows shorter t_{comb} than PF3 at ω = 1500 rpm and P_{PF} = 1000 bar, which is due to higher HRR_{peak} during Stage **I** between θ_1 and θ_2 (see Fig. 2), as shown in Fig. 3(a). The PF1 has more time available to entrain a greater amount of premixed methane-air mixture and burn it during Stage **I**. Therefore, PF1 shows higher η_{comb} (see Table 5) with lower UB-CH_4, THC and CO compared to PF3. On the other hand, PF1 produces higher NO_x and CO_2 due to the higher amount of fuel burned, leading to higher combustion temperatures at ω = 1500 rpm and P_{PF} = 1000, as shown in Fig. 5.

It is recognized that at high pilot-fuel injection pressure, combustion efficiency increases as a result of improved spray characteristics and shorter combustion duration [47–49]. In this case study, both pilot fuels are observed to illustrate similar combustion behavior at P_{PF} of 1500 bar. However, when comparing PF1 with PF3 in Fig. 3(b), PF1 does not exhibit a higher HRR_{peak} than PF3 during Stage **I**, as it depicts at P_{PF} of 1000 bar in Fig. 3(a). Conversely, PF3 shows higher HRR_{peak} during Stages **II** and **III**. It seems that at 1500 bar, PF1 produces locally overlean mixtures due to faster evaporation, prompted by lower viscosity and density, as well as higher volatility. Consequently, lower CN and the small pilot quantity of PF1 lead to an incomplete combustion. Therefore, compared to PF1, PF3 produces higher η_{comb} and AccQ, with lower UB-CH_4, THC, and CO, accompanied by higher NO_x and CO_2 emissions at ω = 1500 rpm and P_{PF} = 1500 bar.

In general, a change in engine speed directly affects overall combustion performance. At a lower engine speed, time per CAD (t_{CAD})[2] increases, thus burning a greater amount of fuel per CAD. It is evident from Figs. 3–5 that at 950 rpm, DF combustion achieves significantly higher combustion rates, shorter t_{ID} and t_{comb}, as well as lower emissions compared to that at 1500 rpm. This decrease in t_{ID} is due to a reduced level of turbulence and a longer residence time, both of which induce higher rates of chemical reactions during pre-ignition processes [50,51]. The decrease in t_{comb} resulted from improved η_{comb} and higher amount of fuel energy released (AccQ) at 950 rpm. It is interesting to note that t_{comb} expressed in units of time (ms) is comparable for both engine speeds. Aside from this, when comparing PF1 with PF3 at 950 rpm in Fig. 3(c) or (d), it is noted that both fuels exhibit similar combustion behavior during Stage **I** as it is observed at 1500 rpm in Fig. 3(a). PF1 causes higher HRR_{peak} during Stage **I** due to lower CN. However, PF3 shows higher HRR_{peak} than PF1 during Stage **III** (i.e. the major part of the combustion) although PF1 has higher volatility (it is suggested that high volatility helps aromatics evaporate faster). This most likely resulted from the higher CN of PF3, which helps aromatic content to efficiently burn at longer t_{CAD} and higher P_{PF}, thereby contributing to the burning of the premixed methane-air mixture during Stages **II** and **III** (more details in Section 3.2). Thus, PF3 causes shorter t_{comb}, higher η_{comb} as well as lower UB-CH_4, THC, and CO (Fig. 5) at the expense of higher NO_x and CO_2 at 950 rpm.

Furthermore, it is observed that at ω = 950 rpm and P_{PF} = 1500 bar, t_{comb} increases despite the higher injection pressure, as shown in Fig. 4 (a). This indicates a long tail combustion during the low-intensity regime of Stage **III**. The heat release rate becomes slower near θ_{90}, causing the overall t_{comb} to become longer than that observed at P_{PF} of 1000 bar. It is noted that the HRR trends in Fig. 3(d) are nearly similar, and that both PFs completely burn in premixed mode during Stage **I** leading to an overlap between θ_2 and θ_{3a}. It seems that PF1 at ω = 950 rpm and P_{PF} = 1500 bar does not produce overlean mixtures due to the lower level of turbulence. However, PF3 causes a marginally higher HRR_{peak} during Stage **III** due to higher CN, as explained earlier. The higher CN fuel produces more reactive radicals, thus influencing the kinetics of the whole combustion process [36].

In summary, we observed here that higher cetane number fuel ignites earlier, and generally improves combustion efficiency of DF combustion. In addition, for the investigated pilot injection conditions, combustion becomes sensitive to pilot fuel thermophysical properties and mixture formation during Stage **I**. Furthermore, the effect of pilot fuel properties is minimal at lower engine speed.

3.2. Case B: Effect of aromatic content (AC)

In this case study, PF2 and PF3 are compared to evaluate the effect of aromatic content on DF combustion. Aromatic hydrocarbons are benzene-like ring structures with high boiling points, density, and C/H ratio. In general, aromatic hydrocarbons experience worse thermal decomposition and slower physical processes, such as evaporation, compared to non-aromatic fuels (e.g. paraffins and naphthenes). This leads to the development of locally fuel-rich zones and possibly to high NO_x and PM emissions [36,38,52–54]. In this study, the aromatic content of the PFs is observed to significantly influence the DF combustion characteristics and emissions, as shown in Figs. 6–8.

Fig. 7(a) compares PF2 and PF3 for ignition-delay time and combustion duration. The values of t_{ID} show minor differences for both PFs

[2] At ω = 1500 rpm, t_{CAD} = 0.111 ms, whereas at ω = 950 rpm, t_{CAD} = 0.17544 ms.

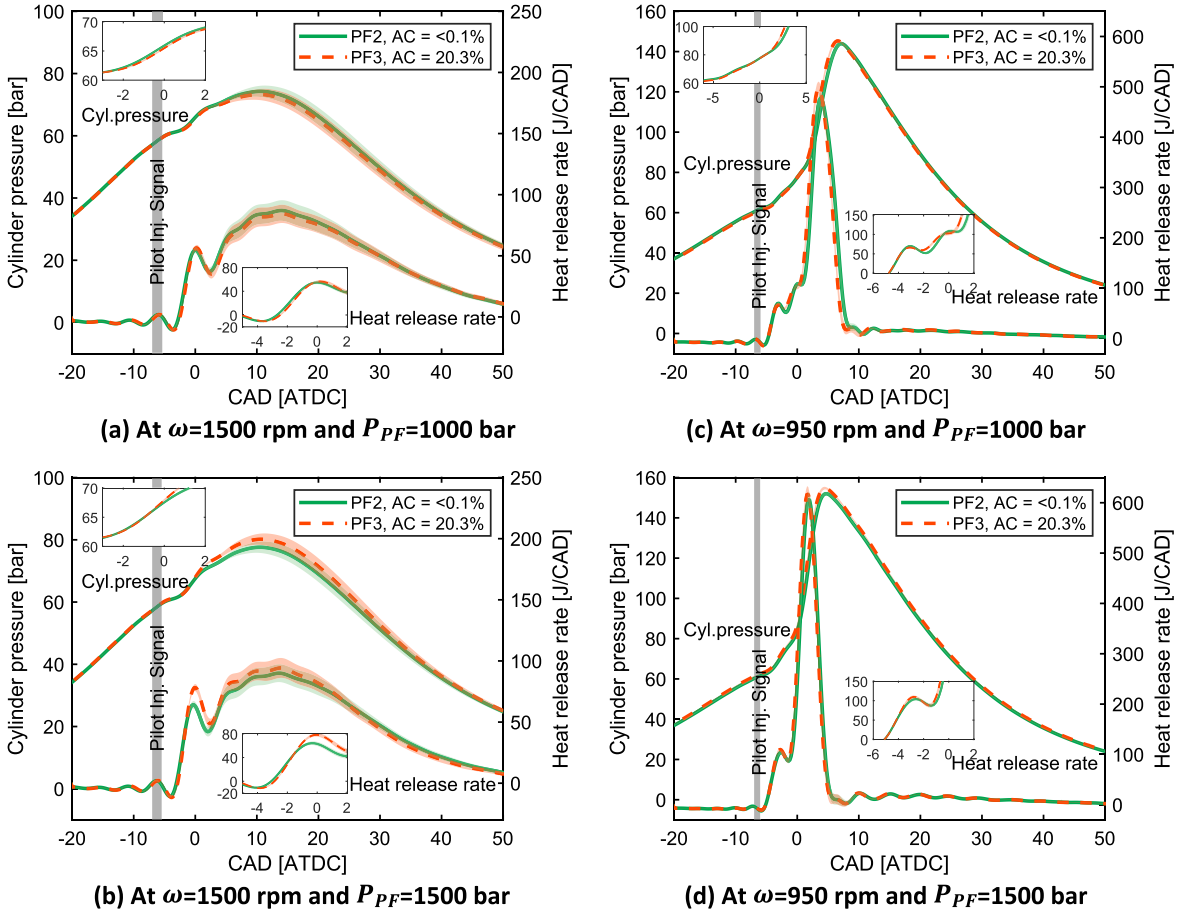

Fig. 6. Averaged cylinder pressure and heat release rate (HRR) data along with standard deviation at two different ω and P_{PF}. Two pilot fuels (PF2 and PF3) are compared to study the effect of AC on lean ($\varnothing_{CH4} = 0.52$) DF combustion.

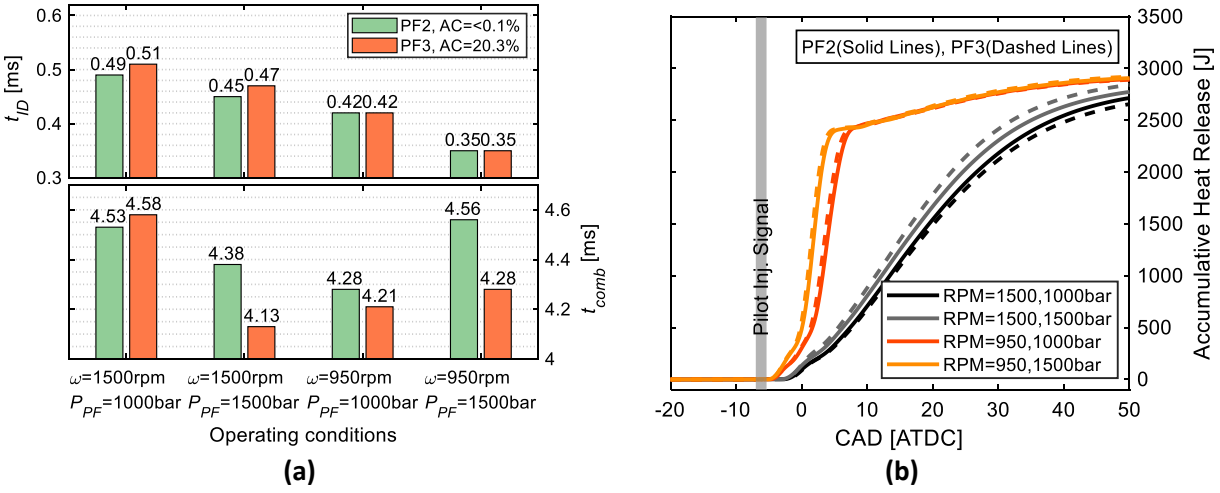

Fig. 7. (a) Ignition-delay time (t_{ID}) and combustion duration (t_{comb}), (b) accumulative heat released (AccQ) data for the study of effect of AC on lean DF combustion.

at corresponding conditions. However, it may be considered that for nearly equal CNs, the values of t_{ID} are same for both PFs. This allows the effect of aromatic content on DF combustion to be examined explicitly. As can be observed from Fig. 6(a), both fuels show similar HRR_{peak} during Stage **I** owing to similar CN. However, PF2 exhibits higher HRR_{peak} than PF3 during Stages **II** and **III** due to the absence of aromatic content. On the other hand, PF3 experiences incomplete combustion due to poor thermal cracking of its aromatic hydrocarbons, leading to weaker premixed methane-air combustion during Stages **II** and **III**. Therefore, PF2 causes higher AccQ and η_{comb} as well as shorter t_{comb} than that observed for PF3 at $\omega = 1500$ rpm and $P_{PF} = 1000$ bar. In addition, PF2 produces lower UB-CH_4, THC and CO at the cost of higher CO_2 and NO_x than PF3 in Fig. 8.

As explained in Section 3.1, combustion efficiency increases at high

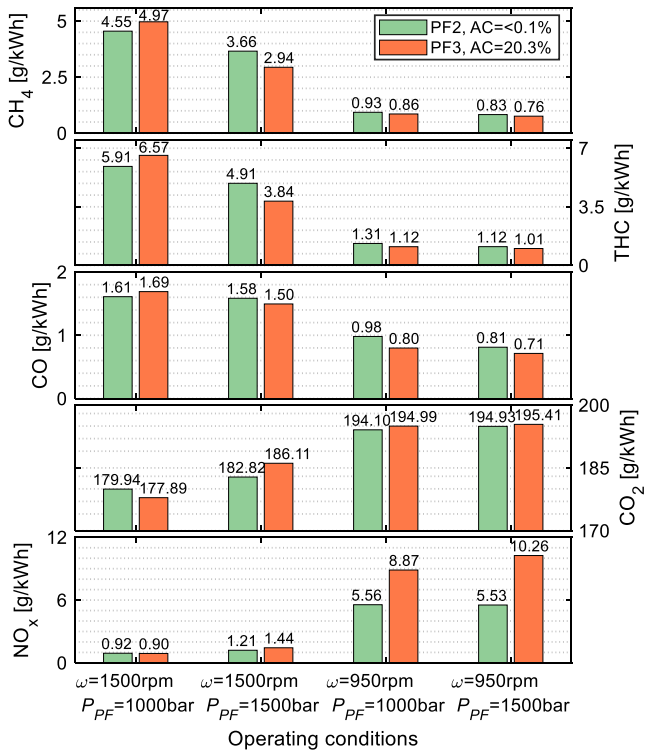

Fig. 8. Engine-out emission data for the study of effect of AC on lean DF combustion.

pilot-fuel injection pressure. Likewise, here PF2 and PF3 show higher η_{comb} at P_{PF} of 1500 bar. However, a comparison of PF2 and PF3 in Fig. 6 (b) reveals that the η_{comb} of PF3 increases more significantly than PF2, leading to an inverse trend than that illustrated in Fig. 6(a). This may be partly due to overlean mixture produced by PF2 and partly due to more rapid evaporation of the aromatic hydrocarbons in PF3 at P_{PF} of 1500 bar. This rapid evaporation causes greater amount of PF3 to burn in premixed mode during Stage **I**, thereby decreasing the probability of PF3 creating locally fuel-rich zones during Stage **II**. Although a comparable amount of PF2 and PF3 burns during Stage **I**, the PF3 produces higher local temperatures because aromatic hydrocarbons are associated with higher adiabatic-flame temperatures [36,38,52–54]. Higher local temperatures may increase the reactivity of the premixed methane-air mixture and intensify HRR_{peak} during Stages **I-III**. Also, high local temperatures from Stage **I** may improve the thermal decomposition of the remaining aromatic hydrocarbons during Stage **II**. Therefore, PF3 results in shorter t_{comb}, higher AccQ as well as lower UB-CH_4, THC and CO with higher η_{comb} than PF2 at $\omega = 1500$ rpm and $P_{PF} = 1500$ bar.

As shown in Fig. 8, PF3 produces significantly higher NO_x than PF2 at comparable η_{comb} due to the presence of aromatic content. This trend increases at higher injection pressure and lower engine speed. Because longer t_{CAD} plays a significant role in achieving higher combustion rates at 950 rpm, the aromatic content of PF3 experiences enhanced thermal decomposition and evaporation at high combustion temperatures than that observed at 1500 rpm. Therefore, PF3 at 950 rpm results in higher η_{comb} with higher peak cylinder pressure and HRR_{peak} than PF2. Furthermore, as described in Section 3.1, t_{comb} is longer at higher P_{PF} of 1500 bar due to long tail combustion occurring during the low-intensity regime of Stage **III**.

Overall, it can be concluded that the presence of aromatic hydrocarbons in a pilot fuel can significantly improve DF combustion efficiency by inducing local high-temperature zones. However, there exists a prominent trade-off between NO_x and UB-CH_4 for a pilot fuel with aromatic content. It should be noted that the burning of aromatic hydrocarbons is mainly dependent on the engine conditions.

3.3. Case C: Combined effect of CN and AC

This case study compares PF1 and PF2 (Figs. 9–11) in order to evaluate the combined effect of cetane number and aromatic content on DF combustion. As described in Section 3.1, a higher cetane number fuel ignites earlier than a lower cetane number fuel. Accordingly, PF2 exhibits shorter ignition-delay time than PF1, as shown in Fig. 10(a). It was demonstrated in the Cases A and B that HRR during Stage **I** is primarily affected by cetane number. While, the aromatic content of a PF generally influences HRR during Stages **II** and **III**. Therefore, in Fig. 9(a), PF1 causes higher HRR_{peak} than PF2 during Stage **I** due to lower CN, while producing lower HRR_{peak} during Stages **II** and **III** owing to the presence of aromatic hydrocarbons. Correspondingly, these trends are reflected in the engine-out emissions at $\omega = 1500$ rpm and $P_{PF} = 1000$ bar in Fig. 11. It is found that PF1 causes lower UB-CH_4 than PF2, which may be attributed to the higher HRR_{peak} during Stage **I**. However, the higher THC and CO produced by PF1 are due to incomplete oxidation (locally fuel-rich zones) of aromatic hydrocarbons during Stage **II**. Despite having higher volatility, PF1 experiences lower combustion rates during Stages **II** and **III**, thus leading to produce lower AccQ, η_{comb} (see Table 5) and CO_2 than PF2 at $\omega = 1500$ rpm and $P_{PF} = 1000$ bar. Also, the relatively shorter t_{comb} caused by PF1 may be attributed to simultaneous higher NO_x and lower AccQ.

It is interesting to note that aromatic hydrocarbons may also affect HRR during Stage **I**, when evaporation or thermal decomposition of aromatic hydrocarbons is enhanced under certain engine conditions. In Fig. 9(b), HRR_{peak} during Stage **I** clearly indicate that higher P_{PF} affects PF1 more favorably than PF2. This may be partly due to overlean mixture produced by PF2 and partly due to burning of aromatic hydrocarbons of PF1 during Stage **I**, as explained in Section 3.2. Consequently, local high temperatures due to combustion of aromatic hydrocarbons help increase HRR during Stages **II** and **III**. Thus, PF1 causes shorter t_{comb} and higher AccQ, η_{comb} and CO_2 than PF2 at P_{PF} of 1500 bar for both engine speeds. Furthermore, PF1 produces lower UB-CH_4, THC and CO than PF2, while higher NO_x are due to higher combustion temperature.

It can be seen from Fig. 9(c) that at 950 rpm PF1 shows same combustion behavior, as illustrated at 1500 rpm in Fig. 9(a). However, the trend of engine-out emissions is slightly different. Here, PF1 is not able to produce lower UB-CH_4 than PF2, which may be attributed to similar extent of HRR during Stage **I**. Also, the difference in THC of both fuels is decreased than that observed at 1500 rpm due to longer t_{CAD} and lower expansion effect around TDC. It is worth to note that at $\omega = 950$ rpm and $P_{PF} = 1000$ bar, PF1 depicts higher η_{th} than PF2, although both fuels show similar η_{comb}. This is due to shorter t_{comb} depicted by PF1.

In brief, it is found out that CN of a fuel directly influences HRR during Stage **I**, while aromatic content of a PF affects HRR during Stages **II** and **III**. Moreover, it is observed that aromatic content of a PF may also affect Stage **I** under certain engine conditions. In comparison, CN has a significant impact on DF combustion as higher CN also helps aromatic content of a PF burn efficiently.

4. Summary of results

Fig. 12 illustrates the energy balance analysis (as described in Section 2.3.1) for all three pilot fuels at various operating conditions. For brevity, the comparison of energy balances is summarized in the single figure to imitate the systematic comparison presented in cases A, B, and C. From figure, it can be clearly seen that compared to combustion efficiency, how much total-fuel energy has converted to useful work denoted as gross indicated efficiency ($\eta_{indicated}$), after dissipating a fraction of combustion energy to pumping, heat transfer and exhaust losses.

In this analysis, it is found that gross indicated efficiency depicts similar trends as illustrated by combustion efficiency. However, at certain operating condition for two comparing fuels, the trend may be slightly different due to heat dissipated in pumping, heat transfer and

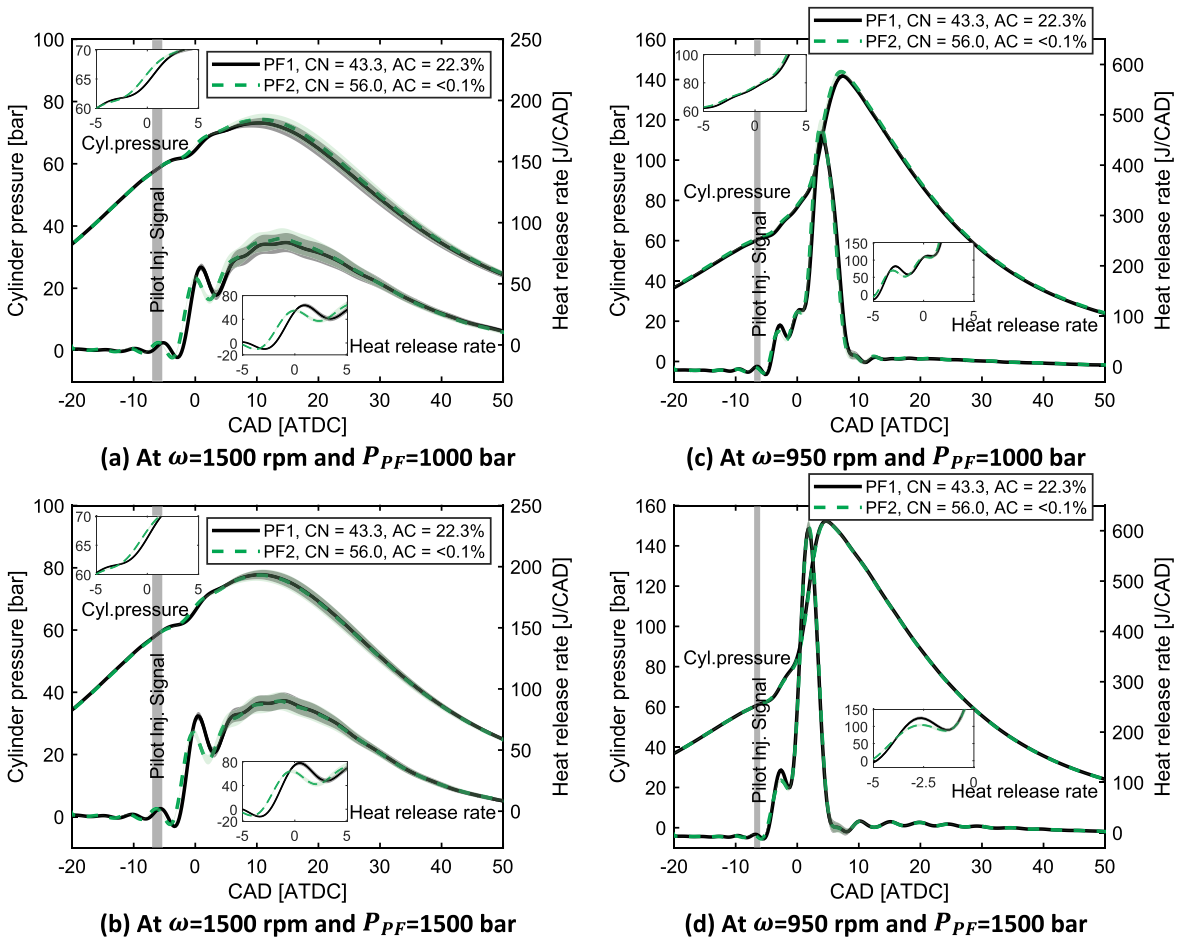

Fig. 9. Averaged cylinder pressure and heat release rate (HRR) data along with standard deviation at two different ω and P_{PF}. Two pilot fuels (PF1 and PF2) are compared to study the combined effect of CN and AC on lean ($\varnothing_{CH4} = 0.52$) DF combustion.

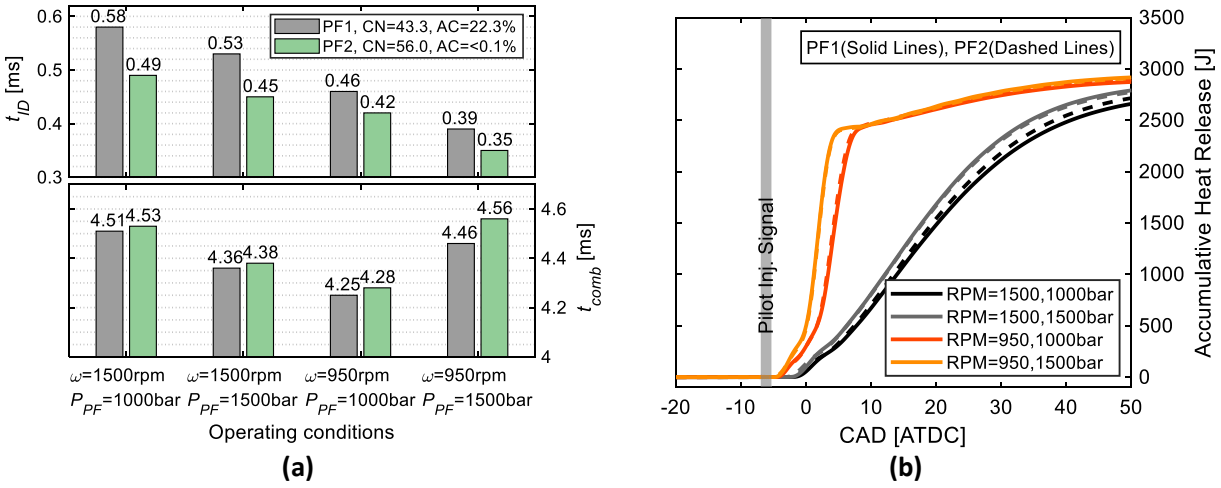

Fig. 10. (a) Ignition-delay time (t_{ID}) and combustion duration (t_{comb}), (b) accumulative heat released (AccQ) data for the study of combined effect of CN and AC on lean DF combustion.

exhaust losses. For example, at $\omega = 1500$ rpm and $P_{PF} = 1000$, PF1 shows higher η_{comb} than PF3. However, owing to higher exhaust and heat transfer losses, PF1 shows slightly lower $\eta_{indicated}$ and η_{th} than PF3. Aside from this, other cases show similar trends for η_{comb} and $\eta_{indicated}$ in this study. Moreover, it seems that the effect of pilot fuels properties is minimal at lower engine speed.

Thus, in following, Tables 6 and 7 summarizes the outcomes of the complete study based on the energy balance analysis, results and averaged trends observed for all three cases A, B, and C.

Additionally, from all three cases A, B, and C, it is also interesting to note that for 950 rpm the NO_x formation level is significantly high particularly for PF1 and PF3. According to the protocol of International

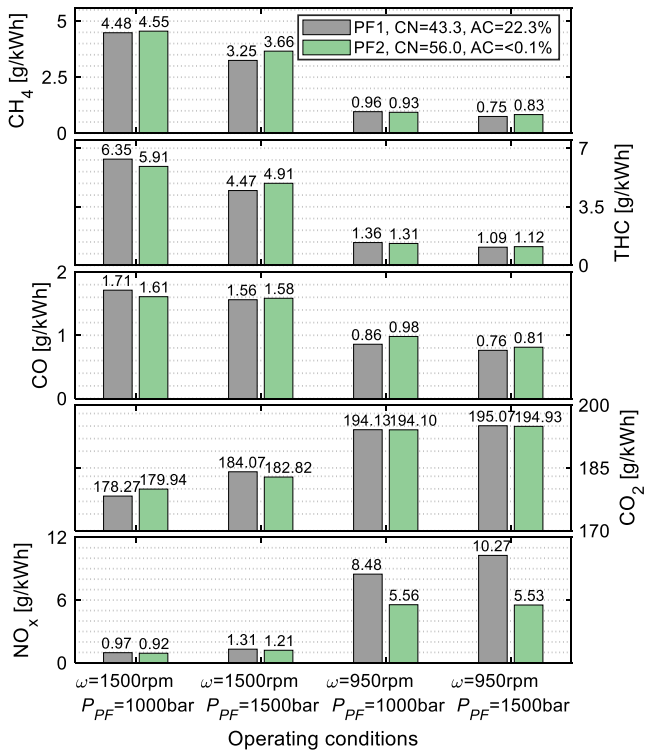

Fig. 11. Engine-out emission data for the study of combined effect of CN and AC on lean DF combustion.

Maritime Agency (IMO), MARPOL Annex VI, the formed NO_x level is even greater than allowed NO_x level for Tier II (for ships constructed after 1st January 2011) and Tier III (for ships constructed after 1st January 2016), which is approx. 9.09 g/kWh and 2.28 g/kWh at 950 rpm, respectively [55,56]. However, for 1500 rpm, the NO_x formation level is lower than allowed levels for both Tiers II and III. The reasons for high NO_x formation level at 950 rpm are high pilot-fuel injection pressure, longer time available per CAD, and the presence of aromatic hydrocarbons in pilot fuels.

5. Conclusions

This study presents the effect of pilot fuel properties on diesel-methane dual fuel (DF) combustion. In particular, the properties of

Table 7
Summary of the averaged trends observed in the complete study for PF properties e.g., CN, AC, volatility, viscosity and density.

Fuel properties	η_{comb}	t_{ID}	t_{comb}	UB-CH_4	THC	CO	NO_x
Cetane number (CN)	↑	↓	↓	↓	↓	↓	↑
Aromatic content (AC)	↑	O	↓	↓	↓	↓	↑
Volatility (T_{10}, T_{50}, T_{95})	O	↓	O	O	O	O	O
Density, Viscosity	O	O	O	O	O	O	O

↑: increases with an increase in fuel property
↓: decreases with an increase in fuel property
O: no change or no strong relationship is observed
Few absolute trends can be different from above averaged trends for certain engine condition.

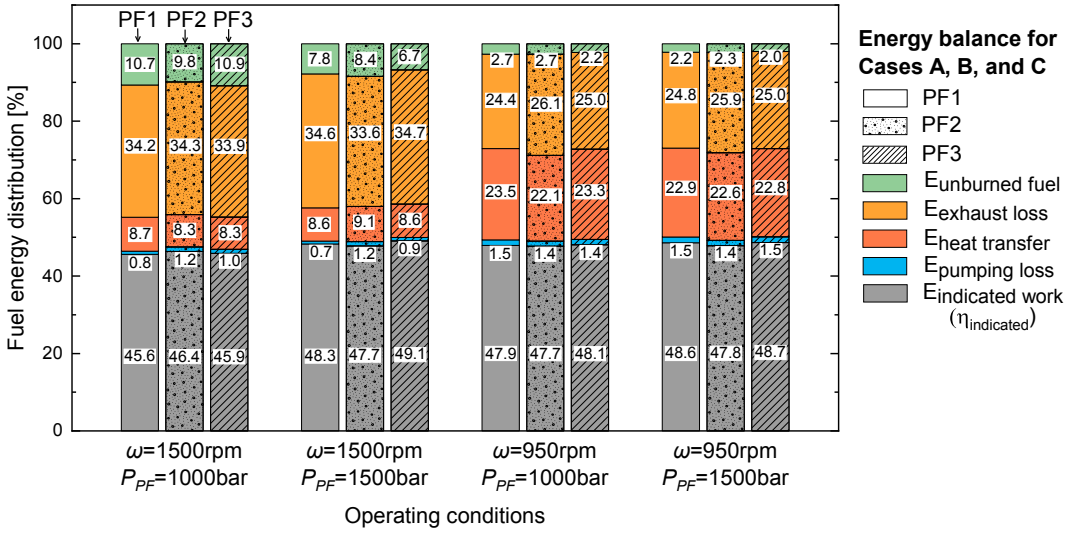

Fig. 12. Energy balance analysis; a comparison of total-fuel energy (TFE) distribution for the all three cases A, B, and C.

Table 6
Summary of the main results from all three Cases A, B, and C.

Test conditions	Combustion efficiency			Stage I HRR_{peak}			Stages II and III HRR_{peak}		
	PF1	PF2	PF3	PF1	PF2	PF3	PF1	PF2	PF3
ω = 1500 rpm and P_{PF} = 1000 bar	+/−	+	−	+	−	−	−	+	−
ω = 1500 rpm and P_{PF} = 1500 bar	+/−	−	+	+	−	+	−	−	+
ω = 950 rpm and P_{PF} = 1000 bar	+/−	−	+	+	−	−	−	+/−	+
ω = 950 rpm and P_{PF} = 1500 bar	+/−	−	+	+	−	−	−	−	+

+: high
+/−: middle
−: low

three diesel-like pilot fuels (PF1, PF2, and PF3) are compared to investigate the influence of cetane number (CN = 43–56), aromaticity (AC = 0–22%) and physical properties on lean DF combustion. The experiments are performed in a single-cylinder full-metal research engine for two pilot-fuel injection pressures at two different engine speeds. For the experiments, the total-fuel energy is kept constant while 97% of the total energy is coming from methane. The remaining 3% of the energy is provided by a pilot fuel to ignite the lean ($\varnothing_{CH4}$ = 0.52) premixed methane-air mixture. The main findings of the present work are concluded below.

1. At equal aromaticity,
   a. A higher CN fuel (PF3) generally improves DF combustion efficiency and causes lower emissions of UB-CH_4 (methane slip), THC and CO than a lower CN fuel (PF1).
   b. Under certain engine conditions, a lower CN fuel may improve combustion efficiency, when: (1) the lower CN fuel is not leaned out, and (2) aromatic hydrocarbons of the higher CN fuel burn inefficiently.
2. At equal cetane number,
   a. A fuel with aromatic content (PF3) typically causes higher combustion efficiency than a non-aromatic fuel (PF2) by inducing higher local temperatures during Stages **II** and **III**, which leads to lower emissions of UB-CH_4 at the expense of higher NO_x.
   b. A non-aromatic fuel may show higher combustion efficiency than a fuel with aromatic content, when the contribution of the aromatic hydrocarbons to the combustion is insignificant.
3. Cetane number and volatility affect the peak heat-release rate during Stage **I**, whereas aromatic content affects the peak heat-release rate during Stages **II** and **III**.
4. At higher pilot-fuel injection pressure, a fuel with lower viscosity, lower density, and lower distillation temperature is more prone to lean out in lean premixed methane-air mixture. On the other hand, aromatic hydrocarbons burn efficiently due to improved mixing. It was found that at higher injection pressure, even with lower CN (PF1), the burning of aromatic hydrocarbons may lead to higher combustion (η_{comb}), gross indicated ($\eta_{indicated}$) and thermal efficiencies (η_{th}) than a higher CN non-aromatic fuel (PF2).
5. At lower engine speed, combustion rates are significantly higher due to longer time available per CAD (t_{CAD}). In addition, longer t_{CAD} enhances thermal decomposition of aromatic hydrocarbons.

These observations reveal that for small quantities of a pilot fuel, generally higher cetane number fuel with higher aromatic content improves DF combustion. In addition, high viscosity, high density, and high distillation temperature avoid the possible leaning out of a pilot spray. Based on the averaged performance trends, the investigated pilot fuels can be rated as PF3 > PF1 > PF2.

CRediT authorship contribution statement

Zeeshan Ahmad: Investigation, Validation, Methodology, Formal analysis, Visualization, Writing - original draft, Writing - review & editing. **Ossi Kaario:** Conceptualization, Resources, Writing - review & editing, Supervision. **Cheng Qiang:** Investigation, Validation. **Martti Larmi:** Supervision, Funding acquisition.

Declaration of Competing Interest

The authors declare that they have no known competing financial interests or personal relationships that could have appeared to influence the work reported in this paper.

Acknowledgment

The Academy of Finland (grant number 13297248) and Fortum-Neste Foundation (grant number 20190102) have financially supported the present work. In addition, the funding from European Union HERCULES-2 project within Horizon 2020 research and innovation programme under grant agreement No. 634135 is acknowledged.

References

[1] BP statistical review of world energy 68th edition; 2019. https://www.bp.com/content/dam/bp/business-sites/en/global/corporate/pdfs/energy-economics/statistical-review/bp-stats-review-2019-full-report.pdf [accessed February 25, 2020].
[2] Varuvel EG, Mrad N, Tazerout M, Aloui F. Experimental analysis of biofuel as an alternative fuel for diesel engines. Appl Energy 2012;1(94):224–31. https://doi.org/10.1016/j.apenergy.2012.01.067.
[3] Bergthorson JM, Thomson MJ. A review of the combustion and emissions properties of advanced transportation biofuels and their impact on existing and future engines. Renew Sustain Energy Rev 2015;1(42):1393–417. https://doi.org/10.1016/j.rser.2014.10.034.
[4] BP (June 11, 2019). Global biofuel production from 2000 to 2018 (in thousand metric tons of oil equivalent) [Graph]. In Statista. Retrieved February 25, 2020, from https://www.statista.com/statistics/274163/global-biofuel-production-in-oil-equivalent/.
[5] Transport sector energy consumption. https://www.eia.gov/outlooks/ieo/pdf/transportation.pdf [accessed February 22, 2020].
[6] Electrification of transport system. https://ec.europa.eu/programmes/horizon2020/en/news/electrification-transport-system-expert-group-report-0 [accessed February 21, 2020].
[7] UNCTAD. Review of maritime transport 2019. Technical report, Geneva. https://unctad.org/en/PublicationsLibrary/rmt2019_en.pdf [accessed February 27, 2020].
[8] Guerry ES, Raihan MS, Srinivasan KK, Krishnan SR, Sohail A. Injection timing effects on partially premixed diesel–methane dual fuel low temperature combustion. Appl Energy 2016;15(162):99–113. https://doi.org/10.1016/j.apenergy.2015.10.085.
[9] Karim GA. Dual-fuel diesel engines. CRC Press; 2015. p. 1–312. https://doi.org/10.1201/b18163.
[10] Srinivasan KK, Agarwal AK, Krishnan SR, Mulone V. Natural gas engines: for transportation and power generation. Springer; 2018. https://doi.org/10.1007/978-981-13-3307-1.
[11] Pachiannan T, Zhong W, Rajkumar S, He Z, Leng X, Wang Q. A literature review of fuel effects on performance and emission characteristics of low-temperature combustion strategies. Appl Energy 2019;1(251):113380. https://doi.org/10.1016/j.apenergy.2019.113380.
[12] Johnson DR, Heltzel R, Nix AC, Clark N, Darzi M. Greenhouse gas emissions and fuel efficiency of in-use high horsepower diesel, dual fuel, and natural gas engines for unconventional well development. Appl Energy 2017;15(206):739–50. https://doi.org/10.1016/j.apenergy.2017.08.234.
[13] Saleh HE. Effect of variation in LPG composition on emissions and performance in a dual fuel diesel engine. Fuel 2008;87(13–14):3031–9. https://doi.org/10.1016/j.fuel.2008.04.007.
[14] Liu J, Yang F, Wang H, Ouyang M, Hao S. Effects of pilot fuel quantity on the emissions characteristics of a CNG/diesel dual fuel engine with optimized pilot injection timing. Appl Energy 2013;1(110):201–6. https://doi.org/10.1016/j.apenergy.2013.03.024.
[15] Ryu K. Effects of pilot injection timing on the combustion and emissions characteristics in a diesel engine using biodiesel–CNG dual fuel. Appl Energy 2013;1(111):721–30. https://doi.org/10.1016/j.apenergy.2013.05.046.
[16] Thomson H, Corbett JJ, Winebrake JJ. Natural gas as a marine fuel. Energy Policy 2015;1(87):153–67. https://doi.org/10.1016/j.enpol.2015.08.027.
[17] Alla GA, Soliman HA, Badr OA, Rabbo MA. Effect of pilot fuel quantity on the performance of a dual fuel engine. Energy Convers Manage 2000;41(6):559–72. https://doi.org/10.1016/S0196-8904(99)00124-7.
[18] Cheng Q, Ahmad Z, Kaario O, Martti L. Cycle-to-cycle variations of dual-fuel combustion in an optically accessible engine. Appl Energy 2019;15(254):113611. https://doi.org/10.1016/j.apenergy.2019.113611.
[19] Kahila H, Kaario O, Ahmad Z, Masouleh MG, Tekgül B, Larmi M, et al. A large-eddy simulation study on the influence of diesel pilot spray quantity on methane-air flame initiation. Combust Flame 2019;1(206):506–21. https://doi.org/10.1016/j.combustflame.2019.05.025.
[20] Shim E, Park H, Bae C. Intake air strategy for low HC and CO emissions in dual-fuel (CNG-diesel) premixed charge compression ignition engine. Appl Energy 2018 Sep;1(225):1068–77. https://doi.org/10.1016/j.apenergy.2018.05.060.
[21] Ushakov S, Stenersen D, Einang PM. Methane slip from gas fuelled ships: a comprehensive summary based on measurement data. J Mar Sci Technol 2019;1:1–8. https://doi.org/10.1007/s00773-018-00622-z.
[22] Ahmad Z, Kaario O, Cheng Q, Larmi M. Impact of ethane enrichment on diesel-methane dual-fuel combustion. SAE technical paper; 2020. https://doi.org/10.4271/2020-01-0305.
[23] Vermeulen RJ. Emissions testing of a Euro VI LNG-diesel dual fuel truck in the Netherlands. Den Haag: TNO; 2019. uuid:1a455afb-ac09-477e-a851-112904eb3384.
[24] Namasivayam AM, Crookes RJ, Korakianitis T, Olsen J. Assessment of combustion in natural gas dual-fuelled compression ignition engines with dimethyl ether and rapeseed methyl ester pilot ignition. Int J Engine Res 2009;10(3):165–74. https://doi.org/10.1243/14680874JER02909.

[25] Namasivayam AM, Korakianitis T, Crookes RJ, Bob-Manuel KD, Olsen J. Biodiesel, emulsified biodiesel and dimethyl ether as pilot fuels for natural gas fuelled engines. Appl Energy 2010;87(3):769–78. https://doi.org/10.1016/j.apenergy.2009.09.014.
[26] Bora BJ, Saha UK. Comparative assessment of a biogas run dual fuel diesel engine with rice bran oil methyl ester, pongamia oil methyl ester and palm oil methyl ester as pilot fuels. Renewable Energy 2015;1(81):490–8. https://doi.org/10.1016/j.renene.2015.03.019.
[27] Tira HS, Herreros JM, Tsolakis A, Wyszynski ML. Characteristics of LPG-diesel dual fuelled engine operated with rapeseed methyl ester and gas-to-liquid diesel fuels. Energy 2012;47(1):620–9. https://doi.org/10.1016/j.energy.2012.09.046.
[28] Selim MY, Radwan MS, Saleh HE. Improving the performance of dual fuel engines running on natural gas/LPG by using pilot fuel derived from jojoba seeds. Renewable Energy 2008;33(6):1173–85. https://doi.org/10.1016/j.renene.2007.07.015.
[29] Korakianitis T, Namasivayam AM, Crookes RJ. Diesel and rapeseed methyl ester (RME) pilot fuels for hydrogen and natural gas dual-fuel combustion in compression–ignition engines. Fuel 2011;90(7):2384–95. https://doi.org/10.1016/j.fuel.2011.03.005.
[30] Barik D, Murugan S. Effects of diethyl ether (DEE) injection on combustion performance and emission characteristics of Karanja methyl ester (KME)–biogas fueled dual fuel diesel engine. Fuel 2016;15(164):286–96. https://doi.org/10.1016/j.fuel.2015.09.094.
[31] Tarabet L, Loubar K, Lounici MS, Khiari K, Belmrabet T, Tazerout M. Experimental investigation of DI diesel engine operating with eucalyptus biodiesel/natural gas under dual fuel mode. Fuel 2014;1(133):129–38. https://doi.org/10.1016/j.fuel.2014.05.008.
[32] Yoon SH, Lee CS. Experimental investigation on the combustion and exhaust emission characteristics of biogas–biodiesel dual-fuel combustion in a CI engine. Fuel Process Technol 2011;92(5):992–1000. https://doi.org/10.1016/j.fuproc.2010.12.021.
[33] Ansari E, Menucci T, Shahbakhti M, Naber J. Experimental investigation into effects of high reactive fuel on combustion and emission characteristics of the Diesel-natural gas reactivity controlled compression ignition engine. Appl Energy 2019;1(239):948–56. https://doi.org/10.1016/j.apenergy.2019.01.256.
[34] Chuahy FD, Kokjohn SL. Effects of the direct-injected fuel's physical and chemical properties on dual-fuel combustion. Fuel 2017;1(207):729–40. https://doi.org/10.1016/j.fuel.2017.06.039.
[35] Gunea C, Razavi MR, Karim GA. The effects of pilot fuel quality on dual fuel engine ignition delay. SAE technical paper; 1998. https://doi.org/10.4271/982453.
[36] Richards P. 'Automotive fuels reference book; 2014. ISBN: 978-0-7680-0638-4. SAE International. https://www.sae.org/publications/books/content/r-297/.
[37] Butts RT, Foster DE, Krieger R, Andrie M, Ra Y. Investigation of the effects of cetane number, volatility, and total aromatic content on highly-dilute low temperature diesel combustion. SAE technical paper; 2010. https://doi.org/10.4271/2010-01-0337.
[38] Han M. The effects of synthetically designed diesel fuel properties–cetane number, aromatic content, distillation temperature, on low-temperature diesel combustion. Fuel 2013;1(109):512–9. https://doi.org/10.1016/j.fuel.2013.03.039.
[39] Herranen M, Huhtala K, Vilenius M, Liljenfeldt G. The electro-hydraulic valve actuation (EHVA) for medium speed diesel engines-development steps with simulations and measurements. SAE technical paper; 2007. https://doi.org/10.4271/2007-01-1289.
[40] Jeihouni Y, Pischinger S, Ruhkamp L, Koerfer T. Relationship between fuel properties and sensitivity analysis of non-aromatic and aromatic fuels used in a single cylinder heavy duty diesel engine. SAE technical paper; 2011. https://doi.org/10.4271/2011-01-0333.
[41] Hulkkonen T, Tilli A, Kaario O, Ranta O, Sarjovaara T, Vuorinen V, et al. Late post-injection of biofuel blends in an optical diesel engine: Experimental and theoretical discussion on the inevitable wall-wetting effects on oil dilution. Int J Engine Res 2017;18(7):645–56. https://doi.org/10.1177/1468087416663548.
[42] Liu H, Altan MC. Science and engineering of droplets: fundamentals and applications. Appl Mech Rev 2002;55(1):B16–7. https://doi.org/10.1115/1.1445335.
[43] Guibet JC, Faure-Birchem E. Fuels and engines, vol. 1. Paris: Editions Technip; 1999. ISBN: 978-2710807537.
[44] Heywood JB. Internal combustion engine fundamentals. McGraw-Hill; 1998. p. 930. https://doi.org/10.1036/007028637X.
[45] Wang B, Pamminger M, Wallner T. Impact of fuel and engine operating conditions on efficiency of a heavy duty truck engine running compression ignition mode using energy and exergy analysis. Appl Energy 2019;15(254):113645. https://doi.org/10.1016/j.apenergy.2019.113645.
[46] Ahmad Z, Kaario O, Qiang C, Vuorinen V, Larmi M. A parametric investigation of diesel/methane dual-fuel combustion progression/stages in a heavy-duty optical engine. Appl Energy 2019;1(251):113191. https://doi.org/10.1016/j.apenergy.2019.04.187.
[47] Yang B, Xi C, Wei X, Zeng K, Lai MC. Parametric investigation of natural gas port injection and diesel pilot injection on the combustion and emissions of a turbocharged common rail dual-fuel engine at low load. Appl Energy 2015;1(143):130–7. https://doi.org/10.1016/j.apenergy.2015.01.037.
[48] Ryu K. Effects of pilot injection pressure on the combustion and emissions characteristics in a diesel engine using biodiesel–CNG dual fuel. Energy Convers Manage 2013;1(76):506–16. https://doi.org/10.1016/j.enconman.2013.07.085.
[49] Imperato M, Kaario O, Sarjovaara T, Larmi M. Influence of the in-cylinder gas density and fuel injection pressure on the combustion characteristics in a large-bore diesel engine. Int J Engine Res 2016;17(5):525–33. https://doi.org/10.1177/1468087415589043.
[50] Bolt JA, Henein NA. The effect of some engine variables on ignition delay and other combustion phenomena in a diesel engine. In: Proceedings of the Institution of Mechanical Engineers, Conference Proceedings 1969 Sep (Vol. 184, No. 10, pp. 130–136). Sage UK: London, England: SAGE Publications. https://doi.org/10.1243/PIME_CONF_1969_184_327_02.
[51] Mohammed EK, Nemit-allah MA. Experimental investigations of ignition delay period and performance of a diesel engine operated with Jatropha oil biodiesel. Alex Eng J 2013;52(2):141–9. https://doi.org/10.1016/j.aej.2012.12.006.
[52] An Y, Vedharaj S, Vallinayagam R, Dawood A, Masurier JB, Najafabadi MI, et al. Effect of aromatics on combustion stratification and particulate emissions from low octane gasoline fuels in PPC and HCCI mode. SAE technical paper; 2017. https://doi.org/10.4271/2017-24-0086.
[53] Kidoguchi Y, Yang C, Miwa K. Effects of fuel properties on combustion and emission characteristics of a direct-injection diesel engine. SAE Trans 2000;1:1149–57. https://doi.org/10.4271/2000-01-1851.
[54] Dumitrescu CE, Stuart Neill W, Guo H, Hosseini V, Chippior WL. Fuel property effects on PCCI combustion in a heavy-duty diesel engine. J Eng Gas Turb Power 2012;134(5). https://doi.org/10.1115/1.4005213.
[55] International Maritime Organization (IMO). Nitrogen oxides (NOx) – Regulations 13. http://www.imo.org/en/OurWork/Environment/PollutionPrevention/AirPollution/Pages/Nitrogen-oxides-(NOx)-%E2%80%93-Regulation-13.aspx [accessed September 21, 2020].
[56] Čampara L, Hasanspahić N, Vujičić S. Overview of MARPOL ANNEX VI regulations for prevention of air pollution from marine diesel engines. In: SHS web of conferences 2018 (vol. 58, p. 01004). EDP Sciences. https://doi.org/10.1051/shsconf/20185801004.